Journal of Materials Chemistry A

PAPER

View Article Online
View Journal | View Issue

Cite this: J. Mater. Chem. A, 2017, 5, 1749

Facile synthesis of hierarchical fern leaf-like Sb and its application as an additive-free anode for fast reversible Na-ion storage†

Liying Liang,[a] Yang Xu,[a] Yueliang Li,[b] Huishuang Dong,[c] Min Zhou,[a] Huaping Zhao,[a] Ute Kaiser[b] and Yong Lei*[ac]

Received 1st December 2016
Accepted 7th December 2016

DOI: 10.1039/c6ta10345f

www.rsc.org/MaterialsA

Hierarchical Sb was successfully fabricated *via* a very simple and cost-effective electrochemical deposition method. Morphological and structural characterizations show that the as-prepared Sb has a uniform fern leaf-like structure which is composed of well-crystallized Sb nanoparticles. The formation mechanism of the fern leaf-like Sb was also investigated. The hierarchical Sb exhibits desirable properties for sodium storage, such as high electrical conductivity and large surface area. When used as an additive-free anode for Na-ion batteries, the as-obtained fern leaf-like Sb reveals excellent cycling stability and rate capability. It can afford a high reversible capacity of 589 mA h g^{-1} over 150 cycles at 0.5 A g^{-1} and retain a capacity of 498 mA h g^{-1} at a high rate of 10 A g^{-1}. Furthermore, a full cell constructed using P2-$Na_{2/3}Ni_{1/3}Mn_{2/3}O_2$// fern leaf-like Sb also displays remarkably stable and robust Na-storage performance, which includes a high capacity retention of 70% after 100 cycles at 0.5 A g^{-1} and a large capacity of 370 mA h g^{-1} at 10 A g^{-1}. The excellent electrochemical performance of fern leaf-like Sb can be attributed to its morphological and structural features that ensure fast ion and electron transport and a stable electrode structure.

Introduction

Sodium ion batteries (SIBs) have captured increasing attention as promising alternative energy storage devices, especially for large-scale energy storage systems, owing to their low cost, environmental benignity, and abundant natural Na resources.[1,2] One critical bottleneck at present is to develop efficient SIB anodes which can store large amounts of Na^+ robustly and durably.[3] Metallic Sb has attracted immense interest because of its high theoretical capacity (660 mA h g^{-1}), which is much higher than that of graphite used for commercial LIB anodes.[4] However, implementation of Sb in SIBs is challenging since it suffers from rapid capacity fading and poor rate capability caused by drastic volume expansion/contraction (390%) upon cycling.[5]

In order to address this issue, designing Sb with special structural features is considered to be an efficient strategy in achieving high electrochemical performance and energy density.[6–9] Sb anodes with various nano-structures have been fabricated to show improved Na-ion storage properties, owing to their short ion and electron diffusion pathways, facile strain relaxation, and large electrode/electrolyte contact areas.[10–15] However, nanomaterials are often self-aggregated due to their high surface energy, which reduces their effective contact areas among active materials, additives, and electrolytes, and thus compromise the electrochemical performance.[16] Therefore, it is still a challenge to keep the effective contact areas large and fully realize the advantage of active materials at the nanometer scale. Recently, hierarchical structures, which possess uniform assemblies of nanoscale primary building blocks (*e.g.*, nanoparticles, nanoplates, and nanorods), have captured considerable attention for enhancing the properties of energy storage and conversion, chemical sensing, chromatography, *etc.*[17–23] This multiscale texturization provides a synergistic joining of two different length scales. The nanosized subunits can guarantee their original features, while the microsized structure would provide additional benefits, such as resistance to aggregation, high porosity, and enhanced electrode stability, consequently leading to improved rate capability and cyclability over their nanostructured and bulk counterparts.[17–22] For instance, a hierarchical Sb anode named cypress leaf-like Sb has been successfully fabricated through a chemical replacement reaction between Sb^{3+} and commercial Mg powder.[24] In this hierarchical structure, the void space among the branches of cypress can relieve the volume expansion and provide active sites for sodiation. As an SIB anode, it showed a high reversible capacity of 550 mA h g^{-1} after 120 cycles. However, the rate

[a]Institute of Physics & IMN MacroNano (ZIK), Ilmenau University of Technology, 98693 Ilmenau, Germany. E-mail: yong.lei@tu-ilmenau.de
[b]Central Facility for Electron Microscopy, Electron Microscopy Group of Materials Science, Ulm University, Albert-Einstein-Allee 11, 89081 Ulm, Germany
[c]Institute of Nanochemistry and Nanobiology, School of Environmental and Chemical Engineering, Shanghai University, Shanghai 200444, China

† Electronic supplementary information (ESI) available. See DOI: 10.1039/c6ta10345f

capability is still not satisfactory, in which it only delivered a capacity of 300 mA h g^{-1} at a current density of 3.2 A g^{-1}.

It is reported that the binder-free anode configuration could deliver better rate capability and cycling performance than the conventional electrode architecture.[25–27] Traditional paste-based electrodes (*e.g.*, cypress leaf-like Sb[24]) usually involve the addition of insulating organic binders to inhibit the collapse of the active materials from current collectors, and electrical conductors to maintain the electrode conductivity onto the metal current collectors.[28] Actually, the binders make no contribution to Na storage, and the electrical conductor only contributes to minimal battery performance. In addition, these two components will greatly decrease the energy density of SIBs. Furthermore, the presence of binders generally results in insufficient ion permeation and blocked electron transport, due to the reduced accessible contact area of the active materials and the increased polarization of the electrodes.[25] Therefore, it is highly desirable to develop highly stable hierarchical Sb structures directly grown on current collectors without using any additives, which can not only effectively decrease the weight of the SIB system, but also enhance the energy density of SIBs.[29] Moreover, the direct growth of hierarchical structures on current collectors can ensure convenient ion diffusion pathways and electron transport channels, and guarantee sufficient structural interspaces for accommodating the volume expansion, which can result in satisfactory rate performance.[29]

Electrochemical deposition is one of the best methods to prepare additive-free electrodes.[30–32] This method offers many advantages, including simple and low-cost equipment, possible operation at room temperature, easy scale-up from atomic dimensions to large areas, fast growth rates, high efficiency, and rigid control of film thickness, uniformity and deposition rate.[33] Moreover, the most distinctive advantage of electrodeposition is to fabricate additive-free electrodes with various complicated shapes. Building upon the above points, in this paper, we synthesized a hierarchical Sb structure directly grown on a Ti substrate using one-step electrochemical deposition, which possesses the morphology of a fern leaf. The as-prepared fern leaf-like Sb is composed of well-crystallized Sb nanoparticles. Further investigation of the growth mechanism of fern leaf-like Sb was also carried out. The fern leaf-like Sb exhibits desirable properties for sodium storage, such as high electrical conductivity and large surface area. It was applied as an additive-free Sb anode for SIBs, showing excellent cyclability and rate capability for both Na-ion half and full cells, which can be attributed to its morphological and structural features that can ensure fast ion and electron transport and a stable electrode structure. We believe that the excellent performance of Sb gained here shall attract increasing attention for synthesizing more interesting and efficient hierarchical Sb electrodes without any additives for energy storage devices.

Experimental

Materials synthesis

1. Synthesis of fern leaf-like Sb. 0.0036 mol $SbCl_3$ was dissolved into 100 mL ethylene glycol under vigorous magnetic stirring for 30 min. The fern leaf-like Sb was prepared using an electrodeposition method. The electrodeposition was conducted in a two-electrode cell with Ti foil as the working electrode and Pt foil as the counter electrode at a constant current density of 1.0 mA cm^{-2}. The product was washed with ethanol and deionized water, and dried at 80 °C under vacuum.

2. Synthesis of layered P2-$Na_{2/3}Ni_{1/3}Mn_{2/3}O_2$. The P2-$Na_{2/3}Ni_{1/3}Mn_{2/3}O_2$ was prepared by a co-precipitation method with nickel and manganese nitrates in a stoichiometric amount with respect to sodium hydroxide. Na_2CO_3 was added afterwards as the sodium source. The calcinations were carried out at 600 °C for 4 h and 900 °C for 10 h in air.

3. Synthesis of $Na_3V_2(PO_4)_3$/C. $Na_3V_2(PO_4)_3$/C was prepared by using a typical sol–gel method. Citric acid (0.2627 g), NaOH (0.515 g), NH_4VO_3 (0.9746 g), and $NH_4H_2PO_4$ (1.4375 g) were added into 200 mL deionized water under constant stirring at 80 °C. After several hours, most of the water was evaporated. Then, the solution was dried at 80 °C for 12 h under vacuum. The mixture was then preheated at 300 °C for 4 h and heated at 850 °C for 8 h under a N_2 atmosphere to obtain the $Na_3V_2(PO_4)_3$/C sample.

Materials characterization

The morphology and structure were characterized by using a scanning electron microscope (SEM, Hitachi S4800), a high-resolution transmission electron microscope (HRTEM, FEI Titan 80-300) and an X-ray diffractometer (XRD, Bruker-axs Discover D8 applying Cu Kα (1.54056 Å)).

Electrochemical measurements

The cells were assembled using CR2032 coin-type cells in a glove box filled with nitrogen with a glass fiber separator (Whatman, GFB/55) and an electrolyte solution of 1.0 M $NaClO_4$ in EC : PC (1 : 1 by volume) with the addition of 5% fluoroethylene carbonate (FEC). The half cells were composed of Na metal as both the counter and reference electrodes and fern leaf-like Sb as the working electrode. The mass loading of fern leaf-like Sb is about 0.6 mg cm^{-2}. The full cells were constructed using the fern leaf-like Sb as the negative electrode and P2-$Na_{2/3}Ni_{1/3}Mn_{2/3}O_2$ and $Na_3V_2(PO_4)_3$/C as the positive electrodes, respectively. The galvanostatic charge–discharge tests were performed at various current densities on a LAND-CT2001A test system (Wuhan, China). The cyclic voltammogram (CV) was recorded on a BioLogic VSP potentiostat. Electrochemical impedance spectroscopy (EIS) was also performed on a BioLogic VSP potentiostat with a frequency of 1 MHz to 10 mHz at the charge state (2.0 V). All of these experiments were conducted at room temperature.

P2-$Na_{2/3}Ni_{1/3}Mn_{2/3}O_2$ was prepared by mixing 80% P2-$Na_{2/3}Ni_{1/3}Mn_{2/3}O_2$, 10% acetylene black, and 10% poly (vinylidene fluoride) (PVDF) by weight with an appropriate amount of 1-methyl-2-pyrrolidinone (NMP). The above mixture was pressed onto an aluminum foil which served as a current collector. The cathode was dried at 120 °C in a vacuum for 12 h. The $Na_3V_2(PO_4)_3$/C positive electrode was also prepared using the above steps and mass ratios. These two different full cells have excessive positive electrode mass.

Results and discussion

The crystal structure of the as-prepared Sb sample is revealed by the X-ray diffraction (XRD) pattern. As shown in Fig. 1, except for the reflections of the substrate (Ti), the rest of the diffraction peaks are in good agreement with the rhombohedral Sb phase (JCPDS no. 35-0732), indicating the successful synthesis of a pure crystalline Sb phase.

The morphologies and structures of the as-prepared Sb sample were characterized using scanning electron microscopy (SEM) and transmission electron microscopy (TEM). The low magnification SEM image in Fig. 2a proves the formation of a large number of fern leaf-like Sb structures in a large-area, in which leaf-like Sb is uniformly dispersed on the Ti foil. Fig. 2b reveals leaf-like Sb with an average diameter of about 0.5–1 μm and a length of 1.5–3 μm. These fern leaf-like Sb structures still retain much space among the leaves, forming a porous morphology which can be expected to not only facilitate electrolyte penetration but also offer an extra space to relieve volume changes upon cycling. Fig. 2c and d show the magnified SEM images, in which many nanoparticles can be seen and they irregularly stack together forming a fern leaf-like structure.

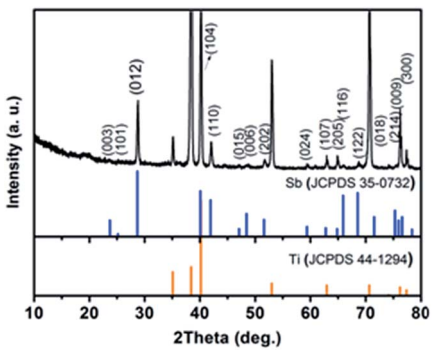

Fig. 1 XRD pattern of fern leaf-like Sb.

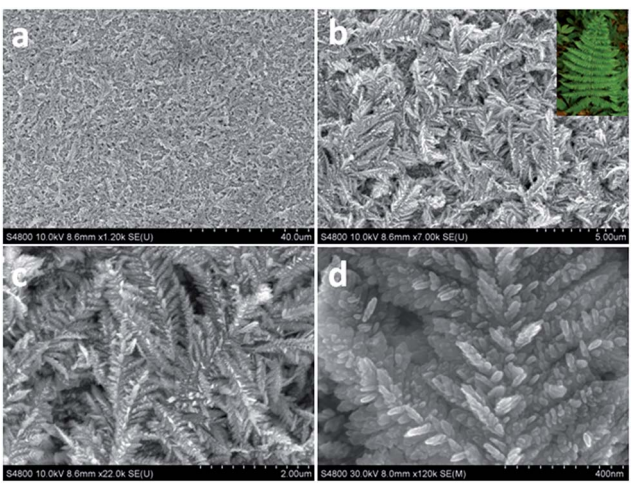

Fig. 2 SEM images of fern leaf-like Sb, ((b) inset) a photo of a fern leaf.

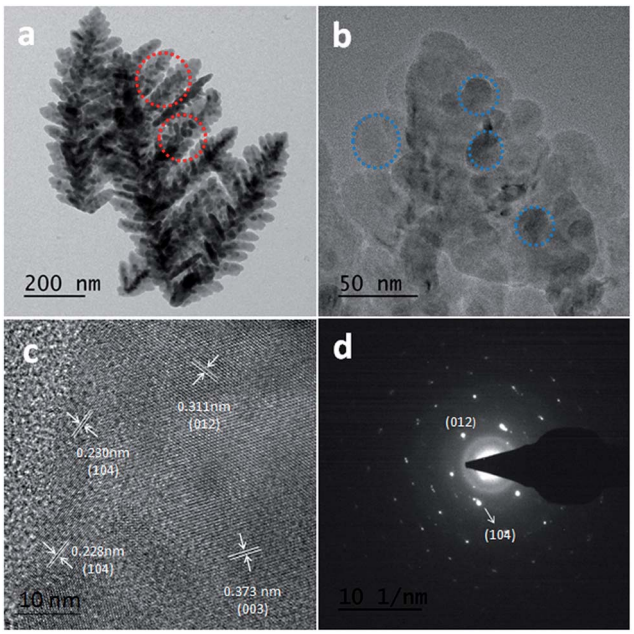

Fig. 3 (a and b) TEM images, (c) HRTEM image, and (d) SAED pattern of fern leaf-like Sb.

The TEM image (Fig. 3a) further presents the well-defined fern leaf-like structure, where the nanoparticles are exhibited in a much clearer way and some are highlighted in red circles. As seen in Fig. 3b, the average size of the nanoparticles is 20–70 nm. The growth scheme of fern leaf-like Sb is illustrated in Fig. S1.† In the initial stage, Sb nanoparticles are observed to uniformly disperse on the Ti foil. With increasing deposition time, due to the strong crystalline anisotropy, Sb nanoparticles directionally aggregated, and the large aggregated particles grew along the preferred growth direction, leading to the formation of the fern leaf-like structure.[24,34–37] The time-dependent morphology is exhibited in Fig. S2.† When the electrodeposition time is 3 min, a large number of nanoparticles are observed (Fig. S2a†), indicating that the preferred morphology is nanoparticles in the initial stage. With the oriented aggregation process continuing, the increasing fern leaf-like structure is formed (Fig. S2b and c†). Finally, well-defined fern leaf-like Sb is obtained (Fig. S2d†). Fig. 3c presents a HRTEM image of this fern leaf-like Sb, where clear lattice fringes can be observed with distances of 3.73, 3.11, and 2.30 Å, corresponding to the (003), (012), and (104) planes of the rhombohedral Sb, further confirming the high crystallinity of the sample. The selected area electron diffraction (SAED) pattern in Fig. 3d proves that the fern leaf-like Sb is polycrystalline.

Motivated by its unique structural features, fern leaf-like Sb was used as an additive-free anode for SIBs. Fig. 4a shows the CV curves of the fern leaf-like Sb in the initial three cycles at a sweep rate of 0.5 mV s^{-1}. In the first cathodic scan, only a strong broad peak located at 0.33 V is observed, which could be attributed to the combination of the formation of a solid electrolyte interface (SEI) layer and Na_xSb alloy which is subsequently transformed into Na_3Sb.[38] During the subsequent cathodic scan, there are three peaks at 0.6, 0.4 and 0.35 V,

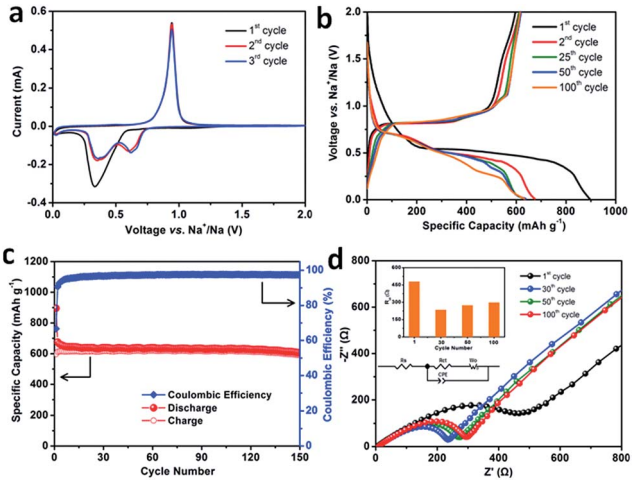

Fig. 4 Electrochemical performance of the fern leaf-like Sb anode. (a) CV curves at a scan rate of 0.5 mV s^{-1} between 0.01 and 2.0 V (*vs.* Na^+/Na). (b) Galvanostatic charge/discharge voltage profiles in different cycles at a current density of 0.5 A g^{-1}. (c) Cycling performance at 0.5 A g^{-1}. (d) Nyquist plots at the charge state (2.0 V) from 1 MHz to 10 mHz.

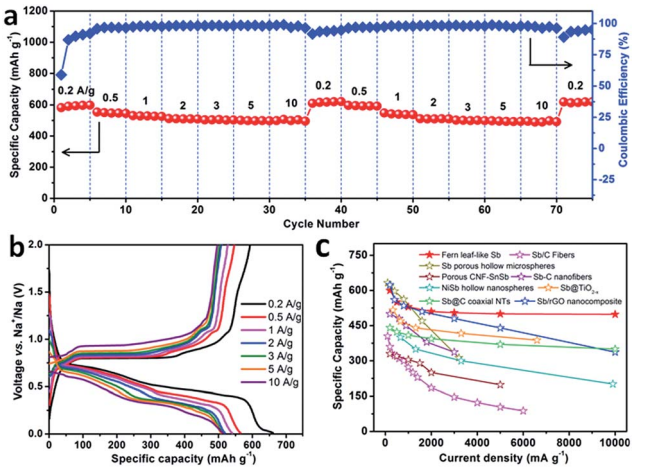

Fig. 5 Electrochemical performance of the fern leaf-like Sb anode. (a) Rate performance at various current densities from 0.1 to 10 A g^{-1}. (b) Charge/discharge voltage profiles at various current densities from 0.1 to 10 A g^{-1}. (c) Ragone plots of the fern leaf-like Sb anode and other Sb-based SIB anodes from the literature (Sb/C fibers,[47] Sb@TiO_{2-x},[48] porous CNF–SnSb,[49] Sb–C nanofibers,[50] NiSb hollow nanospheres,[51] Sb/rGO nanocomposites,[52] Sb@C coaxial NTs,[53] and Sb porous hollow microspheres[14]).

corresponding to the multistep transformation of Sb into a hexagonal Na_3Sb alloy phase by Na-ion insertion. The difference between the first and following cathodic scans is mainly ascribed to the formation of the SEI layer and the rearrangement of the structure.[39] In all of the anodic scans, a strong peak at 0.94 V is clearly observed, resulting from the phase transformation from Na_3Sb to Sb.[38] Fig. 4b shows the charge–discharge curves of fern leaf-like Sb cycled at a current density of 0.5 A g^{-1}, which shows typical characteristics of Sb anodes.[13,38] The voltage profiles with different flat plateaus suggest redox reactions associated with Na alloying and dealloying in the discharge and charge curves, respectively, which is in good agreement with CV results in Fig. 4a. The voltage profiles of both charge and discharge have excellent reproducibility from the 1st to 100th cycles, implying the stable structure of fern leaf-like Sb and high reversibility during cycling.

The cycling performance of the fern leaf-like Sb anode was investigated at a current density of 0.5 A g^{-1}, as revealed in Fig. 4c. The Sb anode presents an excellent cycling stability, and the reversible capacity is 589 mA h g^{-1} after 150 cycles, which is 98.5% of the initial reversible capacity. Except for the initial several cycles, the Coulombic Efficiency (CE) is about 97%, suggesting facile ion and electron transport in this fern leaf-like Sb anode.[40] Table S1† provides the cycling performance comparison of the as-prepared fern leaf-like Sb with some previously reported Sb-based anodes. It is clearly seen that both the capacity and cycle life of fern leaf-like Sb are among the best values for reported Sb-based SIB anodes. The electrochemical sodium storage behaviors of fern leaf-like Sb were further studied by electrochemical impedance spectroscopy (EIS) at different cycles (Fig. 4d). The Nyquist plots contain compressed semicircles in the high frequency region of each spectrum, which refer to the charge transfer resistance (R_{ct}) of the electrode, and inclined lines in the low frequency region, which describe the Na ion diffusion in the electrode–electrolyte interface.[41–43] An equivalent circuit model in the inset of Fig. 4d could be used to fit the impedance data. The resistances R_s and R_{ct} refer to the electrolyte resistance and charge transfer resistance, respectively. The constant phase element CPE and the Warburg element W_o represent double-layer capacitance and the ion diffusion in the host material, respectively.[41–43] The fitting values for charge transfer resistances (R_{ct}) are shown in the inset of Fig. 4d. The large charge transfer resistance (480 Ω) in the high frequency region of the first cycle may be attributed to the influence of the SEI layer.[44] With the increasing cycling numbers, the charge transfer resistances (234 Ω for 30th, 273 Ω for 50th, and 297 Ω for 100th) keep relatively stable only with a minimal increase (inset of Fig. 4d), implying well-maintained electrical contact and a relatively stable SEI layer.[45] These results further prove that the ion diffusion pathways and electron conduction in the electrode were well maintained and the stable electrode structure well accommodated the large volume changes during charge/discharge cycles.[46]

The rate capability of the fern leaf-like Sb was tested at various current densities from 0.2 to 10 A g^{-1}, as shown in Fig. 5a. The anode affords reversible capacities of 600, 550, 530, 510, 505, 500 and 498 mA h g^{-1} at current densities of 0.2, 0.5, 1.0, 2.0, 3.0, 5.0 and 10 A g^{-1}, respectively. At a rate of 10 A g^{-1}, the charging time is only 3 minutes. Fig. 5b exhibits the corresponding voltage profiles of the anode at various current densities. In spite of the increasing current densities from 0.2 to 10 A g^{-1}, both charge and discharge voltage profiles have quite similar shapes with a minimal increase of the voltage offset. A second round of rate testing was performed to further demonstrate the excellent rate capability of the sample. The capacities are rather stable at each rate, regardless of the rate cycling history. When the rate was returned to 0.2 A g^{-1}, the reversible capacity fully recovered to 610 mA h g^{-1}. The excellent rate

performance indicates that the fern leaf-like Sb has good structural tolerance for repeated alloying/dealloying processes and can endure large rate changes while keeping high energy densities at the same time. To the best of our knowledge, the presented rate capability and specific capacities are among the best results of the reported Sb-based anodes (Fig. 5c).

The excellent electrochemical performance of the fern leaf-like Sb can be attributed to its special structural features. First, the hierarchical Sb structure inhibits the self-aggregation of Sb nanoparticles and ensures that the surface remains uncovered to keep the effective and large contact areas. Therefore, the advantages of Sb nanoparticles can be fully achieved, resulting in short pathways both for Na ions and electrons. Second, the microsized structures contribute to enough void space among the branches, which can relieve the volume change upon cycling and simultaneously offer more active sites for Na^+ ions. Third, metallic Sb with excellent electrical conductivity reacts with Na to form the Na_xSb alloy which is also a good conductor. Therefore, the fern leaf-like Sb can be used as an additive-free anode without the addition of other conductive materials, where these leaves are closely associated with each other, easily transporting electrons from the substrate and forming a powerful conductive network, thereby promoting the efficient functioning of these leaves. Furthermore, the Sb anode shows good structural stability, which still maintained the fern leaf-like morphology even after 100 cycles at a high rate of 0.5 A g^{-1} (Fig. S3†).

To evaluate the feasibility of the fern leaf-like Sb as an additive-free anode in practice, two different full cells were assembled by using two different cathode materials (P2-$Na_{2/3}Ni_{1/3}Mn_{2/3}O_2$ and $Na_3V_2(PO_4)_3$/C). The preparations and characterizations of the cathode materials can be found in Fig. S4–S8.† Fig. 6 presents the electrochemical performances of the fern leaf-like Sb//$Na_{2/3}Ni_{1/3}Mn_{2/3}O_2$ full cell. Fig. 6a shows the CV curves of the full cell, which shows well-defined oxidation and reduction peaks and excellent reproducibility, indicating the good stability of electrode materials again. The cycling performance can be seen in Fig. 6b. The full cell affords a high capacity retention of 70% (based on the anode mass) of the theoretical capacity of Sb (660 mA h g^{-1}) after 100 cycles with a high CE of about 97.5% at 0.5 A g^{-1}.

The full cell also exhibits excellent rate capability, delivering the reversible capacities of 565, 540, 505, 470, 440, 405 and 370 mA h g^{-1} at current densities of 0.2, 0.5, 1.0, 2.0, 3.0, 5.0 and 10 A g^{-1}, respectively, with high CEs (Fig. 6c). When the current density was decreased to 0.2 A g^{-1}, the reversible capacity recovered to 520 mA h g^{-1}, which is 92% of the initial reversible capacity, and kept stable up to 75 cycles. Fig. 6d presents the corresponding voltage profiles of the full cell at various current densities. Both charge and discharge profiles retain similar shapes, regardless of the growing current densities from 0.2 to 10 A g^{-1}. The operation voltages are in the range of 2.5 and 2.8 V. The superior rate capability is attributed to the stable electrode structure. The fern leaf-like Sb//$Na_3V_2(PO_4)_3$/C full cell also presents a high capacity, good cyclability and rate capability (Fig. S9†). The performances of the two full cells are much better than those of reported Sb-based full cells.[48,51,54,55] The above results fully prove that the fern leaf-like Sb anode has strong feasibility for Na-ion storage in practice.

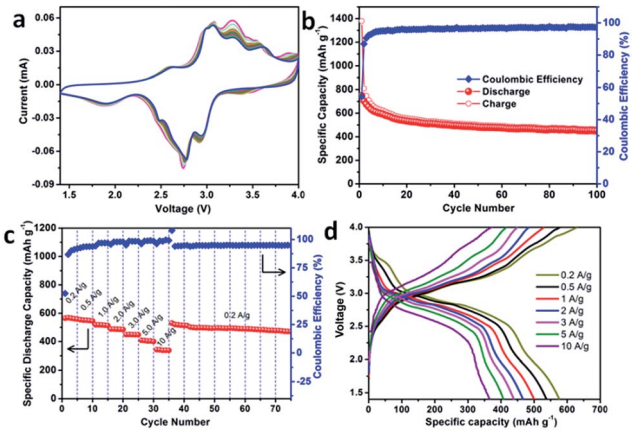

Fig. 6 Electrochemical performance of the fern leaf-like Sb//$Na_{2/3}Ni_{1/3}Mn_{2/3}O_2$ full cell. (a) CV curves at a scan rate of 0.3 mV s^{-1} with 10 cycles. (b) Cycling performance at a current density of 0.5 A g^{-1} (with respect to the anode weight). (c) Rate capability (with respect to the anode weight) at various current densities from 0.2 to 10 A g^{-1}. (d) Charge/discharge voltage profiles at various current densities from 0.2 to 10 A g^{-1}.

Conclusions

In summary, hierarchical Sb was firstly synthesized by using a one-step electrodeposition method, which owns the morphology of a fern leaf. Used as an additive-free anode for Na-ion storage, the obtained fern leaf-like Sb shows excellent cycling stability and rate capability both in Na-ion half cells and full cells. The excellent electrochemical performance can be attributed to the morphological and structural features of the fern leaf-like Sb. It was demonstrated that the fern leaf-like Sb composed of self-assembled nanoparticles not only accommodates the volume expansion, but also facilitates the transport of Na ions and electrons. The synthesis method used in this work for hierarchical Sb structures is cost-effective, simple, and highly efficient, and can be easily scaled up to large areas. We believe that our work may shed light on the scalable fabrication of hierarchical additive-free electrode materials with special morphologies for improved electrochemical performance.

Acknowledgements

This work is financially supported by the European Research Council (ThreeDsurface, 240144), European Research Council (HiNaPc, 737616), BMBF (ZIK-3DNanoDevice, 03Z1MN11), BMBF (Meta-ZIK-BioLithoMorphie, 03Z1M512), German Research Foundation (DFG: LE 2249_4-1), National Natural Science Foundation of China (21577086) and Shanghai Thousand Talent Plan.

Notes and references

1 V. Palomares, P. Serras, I. Villaluenga, K. B. Hueso, J. Carretero-Gonzalez and T. Rojo, *Energy Environ. Sci.*, 2012, **5**, 5884–5901.
2 S. W. Kim, D. H. Seo, X. H. Ma, G. Ceder and K. Kang, *Adv. Energy Mater.*, 2012, **2**, 710–721.
3 S. Y. Hong, Y. Kim, Y. Park, A. Choi, N.-S. Choi and K. T. Lee, *Energy Environ. Sci.*, 2013, **6**, 2067–2081.
4 G. Jeong, Y.-U. Kim, H. Kim, Y.-J. Kim and H.-J. Sohn, *Energy Environ. Sci.*, 2011, **4**, 1986–2002.
5 M. D. Slater, D. Kim, E. Lee and C. S. Johnson, *Adv. Funct. Mater.*, 2013, **23**, 947–958.
6 L. Wu, H. Yu, L. Xiao, X. Ai, H. Yang and Y. Cao, *J. Mater. Chem. A*, 2015, **3**, 5708–5713.
7 Y. N. Ko and Y. C. Kang, *Chem. Commun.*, 2014, **50**, 12322–12324.
8 L. Fan, J. Zhang, J. Cui, Y. Zhu, J. Liang, L. Wang and Y. Qian, *J. Mater. Chem. A*, 2015, **3**, 3276–3280.
9 S. Liu, J. Feng, X. Bian, J. Liu and H. Xu, *Energy Environ. Sci.*, 2016, **9**, 1229–1236.
10 J. Qian, Y. Chen, L. Wu, Y. Cao, X. Ai and H. Yang, *Chem. Commun.*, 2012, **48**, 7070–7072.
11 N. Li, S. Liao, Y. Sun, H. W. Song and C. X. Wang, *J. Mater. Chem. A*, 2015, **3**, 5820–5828.
12 M. Walter, S. Doswald and M. V. Kovalenko, *J. Mater. Chem. A*, 2016, **4**, 7053–7059.
13 L. Xiao, Y. Cao, J. Xiao, W. Wang, L. Kovarik, Z. Nie and J. Liu, *Chem. Commun.*, 2012, **48**, 3321–3323.
14 N. Zhang, Y. Liu, Y. Lu, X. Han, F. Cheng and J. Chen, *Nano Res.*, 2015, **8**, 3384–3394.
15 M. He, K. Kravchyk, M. Walter and M. V. Kovalenko, *Nano Lett.*, 2014, **14**, 1255–1262.
16 L. Mai, L. Xu, C. Han, X. Xu, Y. Luo, S. Zhao and Y. Zhao, *Nano Lett.*, 2010, **10**, 4750–4755.
17 Y. Wu, C. Cao, J. Zhang, L. Wang, X. Ma and X. Xu, *ACS Appl. Mater. Interfaces*, 2016, **8**, 19567–19572.
18 H. B. Wu, H. Peng and X. W. Lou, *Energy Environ. Sci.*, 2013, **6**, 3619–3626.
19 J. Duay, S. A. Sherrill, Z. Gui, E. Gillette and S. B. Lee, *ACS Nano*, 2013, **7**, 1200–1214.
20 Q. Mahmood, M. G. Kim, S. Yun, S.-M. Bak, X.-Q. Yang, H. S. Shin, W. S. Kim, P. V. Braun and H. S. Park, *Nano Lett.*, 2015, **15**, 2269–2277.
21 N. Wu, Y. Zhang, Y. Wei, H. Liu and H. Wu, *ACS Appl. Mater. Interfaces*, 2016, **8**, 25361–25368.
22 Y. Sun, X. Hu, J. C. Yu, Q. Li, W. Luo, L. Yuan, W. Zhang and Y. Huang, *Energy Environ. Sci.*, 2011, **4**, 2870–2877.
23 L. Zhang, H. B. Wu, Y. Yan, X. Wang and X. W. Lou, *Energy Environ. Sci.*, 2014, **7**, 3302–3306.
24 H. Hou, M. Jing, Y. Zhang, J. Chen, Z. Huang and X. Ji, *J. Mater. Chem. A*, 2015, **3**, 17549–17552.
25 X. Li, J. Yang, Y. Hu, J. Wang, Y. Li, M. Cai, R. Li and X. Sun, *J. Mater. Chem.*, 2012, **22**, 18847–18853.
26 S. Wang, L. Xia, L. Yu, L. Zhang, H. Wang and X. W. Lou, *Adv. Energy Mater.*, 2016, **6**, 1502217–1502224.
27 C. Ban, Z. Wu, D. T. Gillaspie, L. Chen, Y. Yan, J. L. Blackburn and A. C. Dillon, *Adv. Mater.*, 2010, **22**, E145–E149.
28 Y. Idota, T. Kubota, A. Matsufuji, Y. Maekawa and T. Miyasaka, *Science*, 1997, **276**, 1395–1397.
29 L. Zhan, S. Wang, L.-X. Ding, Z. Li and H. Wang, *J. Mater. Chem.*, 2015, **3**, 19711–19717.
30 D. H. Nam, K. S. Hong, S. J. Lim and H. S. Kwon, *J. Power Sources*, 2014, **247**, 423–427.
31 L. Liang, Y. Xu, C. Wang, L. Wen, Y. Fang, Y. Mi, M. Zhou, H. Zhao and Y. Lei, *Energy Environ. Sci.*, 2015, **8**, 2954–2962.
32 K.-S. Hong, D.-H. Nam, S.-J. Lim, D. Sohn, T.-H. Kim and H. Kwon, *ACS Appl. Mater. Interfaces*, 2015, **7**, 17264–17271.
33 I. Zhitomirsky, L. Gal-Or, A. Kohn and H. W. Hennicke, *J. Mater. Sci.*, 1995, **30**, 5307–5312.
34 B. J. Yang, Y. C. Wu, H. M. Hu, C. Li, X. G. Yang and Y. T. Qian, *Mater. Chem. Phys.*, 2005, **92**, 286–289.
35 M. H. Rashid and T. K. Mandal, *J. Phys. Chem. C*, 2007, **111**, 16750–16760.
36 G. Zhang, S. Sun, M. N. Banis, R. Li, M. Cai and X. Sun, *Cryst. Growth Des.*, 2011, **11**, 2493–2499.
37 M. Xu, F. Wang, B. Ding, X. Song and J. Fang, *RSC. Adv.*, 2012, **2**, 2240–2243.
38 A. Darwiche, C. Marino, M. T. Sougrati, B. Fraisse, L. Stievano and L. Monconduit, *J. Am. Chem. Soc.*, 2012, **134**, 20805–20811.
39 X. Zhou, Y. Zhong, M. Yang, M. Hu, J. Wei and Z. Zhou, *Chem. Commun.*, 2014, **50**, 12888–12891.
40 C. He, S. Wu, N. Zhao, C. Shi, E. Liu and J. Li, *ACS Nano*, 2013, **7**, 4459–4469.
41 S. Yang, H. Song and X. Chen, *Electrochem. Commun.*, 2006, **8**, 137–142.
42 Y. N. Ko, S. B. Park, K. Y. Jung and Y. C. Kang, *Nano Lett.*, 2013, **13**, 5462–5466.
43 S. H. Choi and Y. C. Kang, *ChemSusChem*, 2013, **6**, 2111–2116.
44 Q. Li, Z. Li, Z. Zhang, C. Li, J. Ma, C. Wang, X. Ge, S. Dong and L. Yin, *Adv. Energy Mater.*, 2016, **6**, 1600376–1600385.
45 J. Song, Z. Yu, M. L. Gordin, S. Hu, R. Yi, D. Tang, T. Walter, M. Regula, D. Choi, X. Li, A. Manivannan and D. Wang, *Nano Lett.*, 2014, **14**, 6329–6335.
46 X. Jia, Y. Cheng, Y. Lu and F. Wei, *ACS Nano*, 2014, **8**, 9265–9273.
47 Y. Zhu, X. Han, Y. Xu, Y. Liu, S. Zheng, K. Xu, L. Hu and C. Wang, *ACS Nano*, 2013, **7**, 6378–6386.
48 N. Wang, Z. Bai, Y. Qian and J. Yang, *Adv. Mater.*, 2016, **1**, 4126–4133.
49 L. Ji, M. Gu, Y. Shao, X. Li, M. H. Engelhard, B. W. Arey, W. Wang, Z. Nie, J. Xiao, C. Wang, J. G. Zhang and J. Liu, *Adv. Mater.*, 2014, **26**, 2901–2908.
50 L. Wu, X. Hu, J. Qian, F. Pei, F. Wu, R. Mao, X. Ai, H. Yang and Y. Cao, *Energy Environ. Sci.*, 2013, **7**, 323–328.
51 J. Liu, Z. Yang, J. Wang, L. Gu, J. Maier and Y. Yu, *Nano Energy*, 2015, **16**, 389–398.

52 W. Zhang, Y. Liu, C. Chen, Z. Li, Y. Huang and X. Hu, *Small*, 2015, **11**, 3822–3829.
53 Z. Liu, X.-Y. Yu, X. W. Lou and U. Paik, *Energy Environ. Sci.*, 2016, **9**, 2314–2318.
54 I. Hasa, S. Passerini and J. Hassoun, *RSC Adv.*, 2015, **4**, 48928–48934.
55 D. Y. W. Yu, P. V. Prikhodchenko, C. W. Mason, S. K. Batabyal, J. Gun, S. Sladkevich, A. G. Medvedev and O. Lev, *Nat. Commun.*, 2013, **4**, 2922–2928.